journal of the mechanical behavior of biomedical materials 132 (2022) 105272

Contents lists available at ScienceDirect

Journal of the Mechanical Behavior of Biomedical Materials

journal homepage: www.elsevier.com/locate/jmbbm

Experimental determination of the contact pressures produced by a nasal continuous positive airway pressure mask: A case study

Fabio Savoldi [a,*], Lorenzo Svanetti [b], James K.H. Tsoi [c], Min Gu [a], Corrado Paganelli [b], Francesco Genna [b], Nicola F. Lopomo [d]

[a] Orthodontics, Paediatric Dentistry and Orthodontics, Faculty of Dentistry, The University of Hong Kong, Prince Philip Dental Hospital, 34 Hospital Road, Sai Ying Pun, Hong Kong SAR
[b] Orthodontics, Dental School, Department of Medical Surgical Specialties, Radiological Sciences and Public Health, University of Brescia, Piazzale Spedali Civili 1, 25123, Brescia, Italy
[c] Dental Materials Science, Applied Oral Sciences and Community Dental Care, Faculty of Dentistry, The University of Hong Kong, Prince Philip Dental Hospital, 34 Hospital Road, Sai Ying Pun, Hong Kong SAR
[d] Department of Information Engineering, University of Brescia, Via Branze 38, 25123, Brescia, Italy

ARTICLE INFO

Keywords:
Continuous positive airway pressure
Contact pressure
Pressure ulcers
Obstructive sleep apnoea
Facial growth

ABSTRACT

Background: A continuous positive airway pressure (CPAP) mask is a respiratory ventilation method used for treating breathing disorders including respiratory failure and obstructive sleep apnoea (OSA). The forces applied by a CPAP mask may affect facial development and lead to pressure ulcers. In an experimental setting, the magnitude and the distribution of the contact pressures developed by a CPAP mask on the face were investigated for providing information aiming at optimizing the design of the device.
Materials and methods: A nasal CPAP mask with forehead support was placed via its headgear straps on a rigid phantom head and then a controlled load was incrementally applied via a mechanical testing system (5848 Micro Tester, Instron), up to 4 maximum levels of exerted force, namely 5 N, 10 N, 15 N, and 20 N. Real-time pressure mapping was realized by means of sensor matrixes (I-Scan System, Tekscan) applied on the facial surface in four regions (forehead, nasal bridge, zygoma, and maxilla). The data were then transferred on a virtual model created by 3D scans of both the CPAP mask and the phantom head used in the experiments.
Results: At increasing applied force, increases in average contact pressure were present at the zygomatic region (1–8 kPa), nasal bridge (12–14 kPa), and forehead (13–29 kPa), while the maxillary region showed relatively stable values (9 kPa). Despite the overall increase in average contact pressure with increasing applied force, no direct proportionality was present. Contact areas did not show clear increments, despite force may redistribute on a larger area, as sensors did not cover the entire mask perimeter. Peak contact pressure values were somehow affected by pressure concentrations that led to saturation in some areas of the sensors (up to 2% of the sensels).
Conclusions: The CPAP mask exerts pressures that may be not uniformly distributed on the face of a subject. This information underlines the clinical importance of assessing both the pressure exerted and the areas that are interested by the mask contact, so as to optimise the CPAP masks design for obtaining a good compromise between ventilation performance and reduction of possible side effects on living tissues.

1. Introduction

1.1. Background

Continuous positive airway pressure (CPAP) therapy is a form of non-invasive ventilation (NIV) used to treat various medical conditions that range from acute respiratory failure associated with COVID-19 infection (Nightingale et al., 2020) to chronic obstructive sleep apnoea (OSA) (Lumeng and Chervin, 2008). OSA is a sleep disorder characterised by recurrent episodes of obstruction of the upper airway during sleep that result in greater respiratory efforts with reduction in oxyhaemoglobin saturation, causing sleep fragmentation and multiple symptoms

* Corresponding author.
E-mail addresses: fabiosavoldi@live.com (F. Savoldi), lorenzo.svanetti@gmail.com (L. Svanetti), jkhtsoi@hku.hk (J.K.H. Tsoi), drgumin@hku.hk (M. Gu), corrado.paganelli@unibs.it (C. Paganelli), fgenna988@gmail.com (F. Genna), nicola.lopomo@unibs.it (N.F. Lopomo).

https://doi.org/10.1016/j.jmbbm.2022.105272
Received 4 March 2022; Received in revised form 6 May 2022; Accepted 11 May 2022
Available online 14 May 2022

including daytime sleepiness (Jennum and Riha, 2009). Due to the early onset of paediatric OSA, the need of chronic CPAP treatment, and a prevalence of 1%–4% in the general population, children with this condition may represent a suitable example for the present case study (Lumeng and Chervin, 2008). CPAP ventilators administer air via a facial mask at a clinically effective (*i.e.*, titrated) pressure, which usually ranges from few cm of H_2O to 20 cm of H_2O (Kushida et al., 2008). For example, CPAP treatment is used in children with OSA to allow the mechanical elimination of the obstruction (McArdle et al., 1999) with administration of 8–10 h per night and – in some cases – daytime application (Kushida et al., 2008). CPAP masks can be nasal, oro-nasal, or full-face, and they are available in different shapes for better adaptation to the face, with a headgear constituted by elastic straps that keep the mask in position to limit air leakage (Krieger, 1992). In particular, nasal masks apply pressure on the midface, concentrating the contact on a small area (Schallom et al., 2015; Vaschetto et al., 2014), which is also particularly relevant for facial growth (Li et al., 2000).

In fact, a first aspect to consider in patients undergoing CPAP treatment is the effect of contact pressures on facial hard tissues. The human skull is composed by bones that – in patients with active skeletal growth – may undergo remodelling along the sutures, which are nearly immovable fibrous articulations with a ligament (*i.e.*, a syndesmosis) that connects two bony fronts (Savoldi et al., 2018). Bone remodelling along sutures can be stimulated by the application of mechanical forces (Hierl et al., 2001) and, since the CPAP mask applies forces on the face, previous authors have hypothesised a relationship between the use of CPAP mask and facial deformities in children (Fauroux et al., 2005; Li et al., 2000; Villa et al., 2002). On the contrary, in adults with complete skeletal growth, CPAP mask use may change dental position (Tsuda et al., 2010). In fact, teeth are supported by a periodontal ligament (*i.e.*, a gomphosis) joining the radicular cement with the alveolar bone (Ho et al., 2007), which is subject to bone remodelling under mechanical stimuli, and remains active throughout the whole life (Garlet et al., 2008).

A second aspect to consider is that CPAP masks may also injure soft tissues, as sustained tissue distortion causes direct cell-scale damage and triggers secondary inflammatory damage and tertiary ischaemic damage (Gefen et al., 2020). The incidence of NIV-related pressure ulcers has been shown to range from 5% to 50% for a 2–4 h usage, and up to 100% after 48 h (Carron et al., 2013). In particular, patients using oro-nasal CPAP masks were reported to have higher incidence of skin breakdown compared to those using total face masks (Yamaguti et al., 2014), showing that distributing the forces on a larger area might be beneficial. In addition, cutaneous injuries have been recently reported during CPAP treatment of COVID-19 respiratory failure (Gefen and Ousey, 2020). Thus, knowledge about the contact pressures applied by a CPAP mask is relevant for optimizing their design and reducing unwanted consequences on facial tissues (Ma et al., 2018).

Recent studies have described the pressures generated by the CPAP mask on areas such as the nasal bridge (Brill et al. 2017, 2018; Worsley et al., 2016) and the perinasal region (Worsley et al., 2016). In addition, forces on the cheeks and on the chin have been reported by others (Peko Cohen et al., 2019). Nevertheless, these assessments were carried out without measuring the total force applied on the straps of the headgear. In addition, even though a recent finite element analysis (FEA) simulation provided a broader anatomical assessment (Genna et al., 2022), only few areas interested by CPAP mask pressures have been considered for mechanical assessments so far.

1.2. Objective

The objective of the present case study was to develop a laboratory model to quantitatively estimate the distribution of the pressures exerted by a nasal CPAP mask on the face of a subject. The hypothesis was that contact pressures are not evenly distributed on the different facial regions, reaching levels that may affect bone growth or cause pressure ulcers. Findings will be relevant to develop strategies to minimise the onset of craniofacial deformities and to optimise the mask design for reducing the chance of other iatrogenic effects.

2. Materials and methods

2.1. Materials

A hollow polyvinyl chloride phantom head of natural size for an adult male (circumference of 55 cm (Bushby et al., 1992)) was filled with dental plaster. The head was mounted on a stainless-steel rod connected to a custom-made aluminium frame holding the head and allowing inclination and rotation adjustments for its positioning during mechanical testing. A medium size nasal CPAP mask was used (iVolve N2, BMC Medical, P. R. of China), which was composed by a polycarbonate rigid frame supporting a vinyl-methyl silicone rubber cushion for sealing the interface between the mask and the skin. Further, the mask included an extension of the frame connecting a forehead support provided with a silicon rubber cushion to limit skin damages. The neoprene/nylon headgear was made of two symmetrical 20 mm wide straps (one at the forehead level and one at the nasal level). The straps were made of one layer of unbroken loop fabric on the outer surface, one of styrene butadiene copolymeric rubber in the middle, and one of nylon on the inner surface. Four Velcro connectors were present at the extremity of each strap for tightening the mask on the face (Fig. 1).

2.2. Mechanical testing setup

The aluminium frame was secured to the bottom of the testing machine, and the head was positioned face-down with the main axis perpendicular to the floor. The mask was connected to the headgear and a tensile force was applied to the headgear perpendicularly to the main axis of the head by using a mechanical testing machine (5848 Micro Tester, Instron, Norwood, MA, USA) with a static load cell of ±2000 N. The headgear was connected to the testing machine by a horizontal stainless steel rod and the straps of the headgear were adjusted with Velcro for being uniformly loaded. In a load-controlled configuration, different magnitudes of force were applied (5, 10, 15, and 20 N), with simultaneous acquisition of the contact pressure distributions (Fig. 1).

2.3. Pressure-mapping sensors

Four thin flexible resistive contact pressure mapping sensors with trimmable configuration (model 4201, 45.7 × 21.1 mm matrix, 27.6 sensels/cm^2 resolution, by Tekscan, MA, USA) with dedicated real-time pressure mapping software (I-Scan System, Tekscan, MA, USA) were applied on four different regions of the phantom head for measuring the contact pressures (*i.e.*, forehead, nasal bridge, zygoma, and maxilla). The sampling frequency was 50 Hz, with a mean squared error of 2.7% in the measurements (Brimacombe et al., 2009). Assuming a symmetrical distribution of the forces applied by the mask relatively to the facial midline, sensors were positioned so that results could be mirrored on the opposite side of the face (Fig. 1). The position of each sensor with respect to the phantom head was registered through an opto-electronic system (Smart-DX 400, BTS Bioengineering) with ten digital cameras equipped with infra-red illuminators and reflective passive markers. Seven markers were attached to the head, creating a 3D reference system for the segment. A tracked probe pointer was then used to scan the facial surface and identify the 3D area and position of each sensor with respect to the anatomical segment, so that the output of the sensors matrix could be transferred onto the facial surface.

To obtain pressure distributions, sensors were calibrated before and after data acquisition by using the mechanical testing machine. The procedure was carried out by linear calibration for single array by imposing a known load (*i.e.*, 5, 10, 15, and 20 N), according to specifications from the manufacturer (Tekscan Linear Calibration, Tekscan,

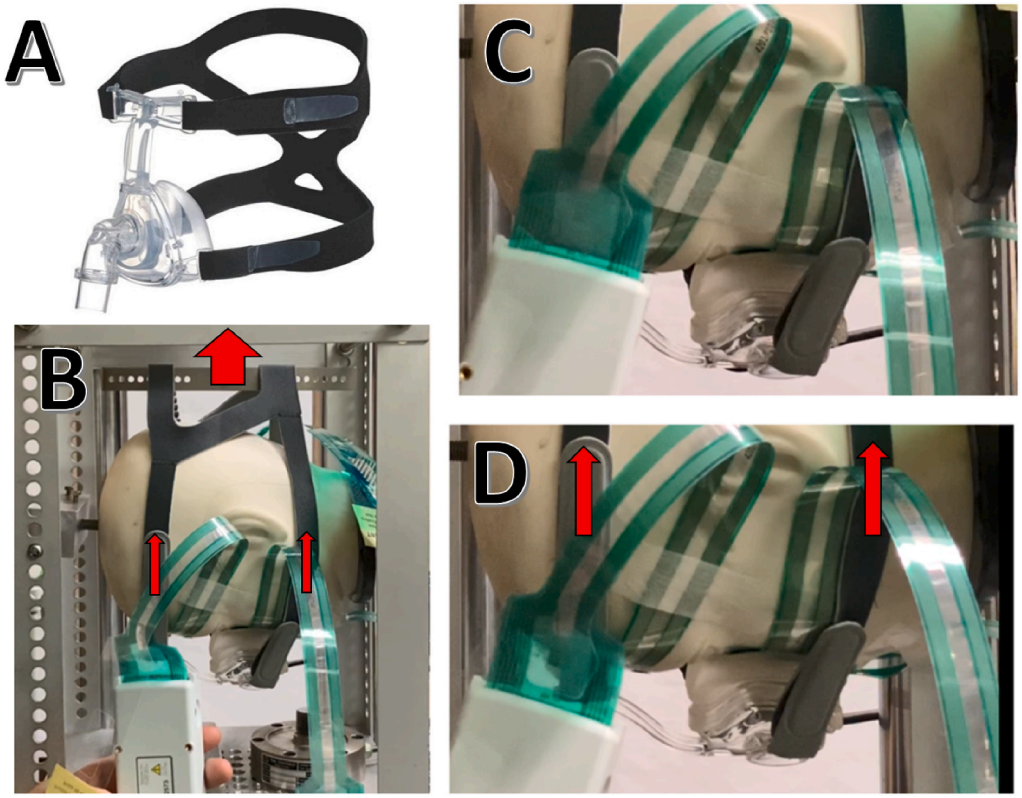

Fig. 1. Setup for the mechanical testing. The continuous positive airway pressure (CPAP) mask with respective headgear straps (**A**). View of the supporting frame and bar that was used for the load application (*red arrows*), with sensors are applied on the facial surface (**B**). View of the CPAP mask before (**C**) and during (**D**) loading, where compression of the silicone cushion can be noticed.

MA, USA). For each sensor, the head was oriented so that the sensor surface was perpendicular to the loading direction, and force was applied through a flat stainless steel tip (Ø = 14.0 mm) covered with 2.0 mm silicon layer. After application on the head surface, sensors configuration was set equal to zero (accounting for possible deformations due to irregular facial profile). Further details about the acquisition of the position of the sensors and their calibration are reported in the **Appendix**.

2.4. Data analysis

The analysis of the contact pressures and contact areas was carried out independently for each facial region (*i.e.*, forehead, nasal bridge, zygoma, and maxilla). The peak contact pressure (kPa) was defined as the maximum contact pressure among all the values recorded by all sensing elements of a sensor matrix. By choosing a threshold of 30% of the saturation value of each single sensor for discriminating "active" from "inactive" elements (pressures smaller than the threshold were considered as "noise"), the active contact pressure area (mm^2) was defined as the sum of the areas of the active elements of a sensor, at the moment in which the peak contact pressure was detected. The average contact pressure (kPa) was calculated as the ratio between the sum of all the contact pressure values recorded in an active area of a sensor at the moment in which the peak contact pressure was detected, and the number of active elements (this variable was introduced to allow an additional estimation that was not based only on peak contact pressures, which can be influenced by surface irregularities and sensor placement, and may be not be clinically relevant). Data were summarised and qualitative comparison was performed among each area, by considering each maximum force applied.

3. Results

Out of 264 sensels for each contact pressure sensor, the saturation of the sensors during data acquisition varied between 0% (0/264, mainly on the nasal bridge) to 2.3% (6/264, mainly on the maxilla), further details are reported in the **Appendix**. Data about peak contact pressure, average contact pressure, and active contact pressure area are presented in Fig. 2.

The forehead region showed increase in average contact pressure (13–29 kPa) and contact pressure area (54–62 mm^2) when the force increased from 5 to 20 N. Average contact pressures were the highest compared to the other regions. No relevant variations in peak contact pressure were observed because of sensor saturation at 55 kPa.

The zygomatic region showed increase in average contact pressure (1–8 kPa) and contact pressure area (40–44 mm^2) when the force increased from 5 to 20 N. This was the region where the smallest average contact pressures were detected. No relevant variations in peak contact pressure were observed because of sensor saturation at 69 kPa.

The nasal bridge region showed increase in average contact pressure (12–14 kPa), but not in contact pressure area (58 mm^2) when the force increased from 5 to 20 N. Average contact pressures had intermediate values compared to the other regions, together with the maxillary region. Small variations in peak contact pressure were observed (22–23 kPa).

The maxillary region showed stable values of average contact pressure (9 kPa) and no clear trend in terms of contact pressure area (up to 228 mm^2) when the force increased from 5 to 20 N. Average contact pressures had intermediate values compared to the other regions, together with the nasal bridge region. No relevant variations in peak contact pressure were observed because of sensor saturation at 23 kPa.

Highest peak pressures were located primarily in the lower area of the zygomatic region (close to the upper area of the maxillary region),

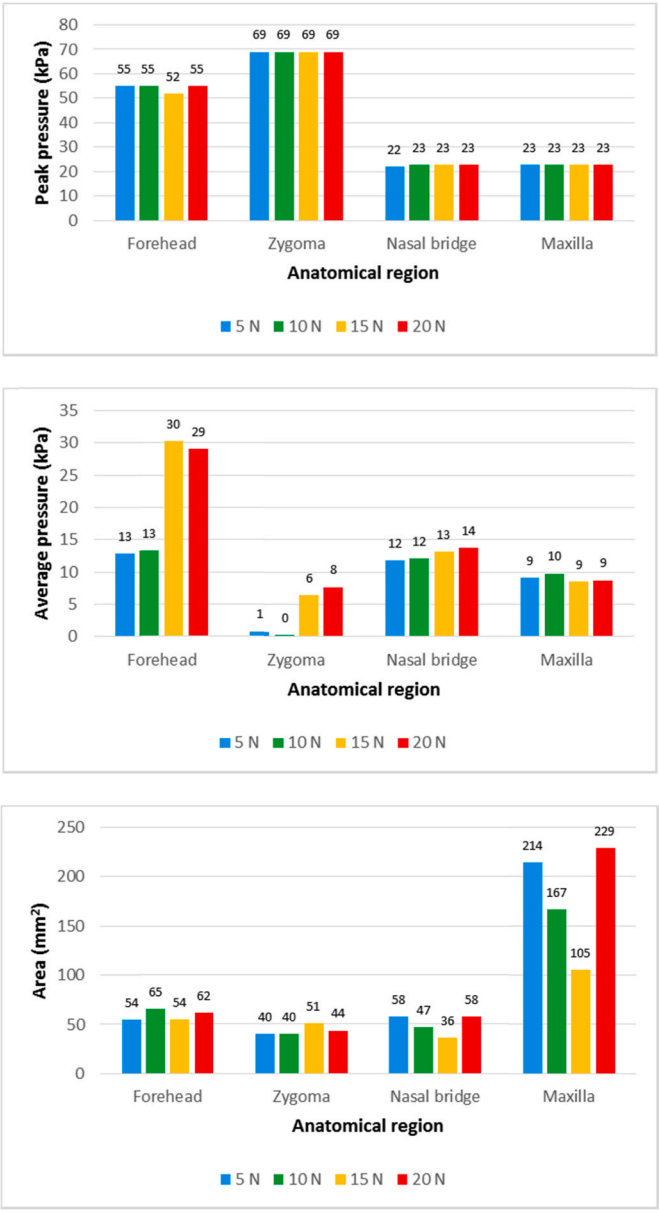

Fig. 2. Peak contact pressure (*top*), average contact pressure (*middle*), and active contact pressure area (*bottom*) for each analysed region, when the continuous positive airway pressure (CPAP) mask was loaded by means of the headgear. Data are presented for each applied force: 5 N (*light blue*), 10 N (*green*), 15 N (*yellow*), and 20 N (*red*), and respective values are reported on top of each column.

and along the contact area of the lower border of frontal cushion in the forehead region. In addition, great variation in peak pressure were present within the same anatomical region, with specific areas of the mask perimeter revealing a high pressure concentration, while others were left almost unloaded (Fig. 3).

4. Discussion

The present experiment showed that the CPAP mask may exert contact pressures that are not uniformly distributed on the face, with the nasal bridge and the forehead region subject to higher average pressures compared to the zygoma and the maxilla. Possible effects of these pressures on the facial growth of young patients constitute a clinically relevant concern that still needs to be addressed (Fauroux et al., 2005; Li et al., 2000; Villa et al., 2002). Most of the knowledge about the magnitude of forces capable of having orthopaedic effects on the head of children comes from studies in dentofacial orthopaedics about the use of headgears applied to the cranial vault and anchored to the maxilla to limit its excessive forward growth (Perillo et al., 2012). For such purpose, forces between 500 and 1500 g (Graber et al., 1985), or 2–12 N (Braun and Bottrel, 2004; Johnson et al., 1999; Lyons and Ramsay, 2002) should be applied. Given that the susceptibility of the craniofacial skeleton to orthopaedic forces is even greater in young children, there is a legitimate concern of possible skull deformations due to CPAP mask usage (Li et al., 2000). In fact, previous authors suggested to avoid prolonged CPAP therapy below that age of twelve (Villa et al., 2002), as the midface completes most of its growth around this age. Overall, growth modification may involve bones that are attached to the cranium via sutures, while the mandible is connected to the skull via a condyle with a synovia (*i.e.*, a condylarthrosis) (Ochoa and Nanda, 2004), which can be safely advanced for enlarging the upper airway (Gu et al., 2021) while compression during retrusion may lead to necrosis. Thus, the magnitude of CPAP forces should be low enough to avoid damages to the mandibular joint, and to avoid restraining the growth of the other craniofacial bones, while maintaining adequate ventilation performance.

Little information is available about the overall force that is used for securing the CPAP mask on the face. One study reported strap tensions between 9.4 and 105.0 gf (0.1 N–1 N) per single strap to maintain a sub-optimal air leakage of 50 l/min (Shikama et al., 2018), representing a total force up to about 4 N (for the four straps) that was similar to the 5 N tension adopted in the present study. Incremental forces up to 20 N were applied in the present experiment to simulate higher tensions that might be needed if leakage of 12 l/min is the clinical target (Fischer et al., 2008). With regard to forces exerted on the face, previous authors reported values of 0.5 N on the cheeks, 2 N on the nasal bridge, and 4 N on the chin (Peko Cohen et al., 2019). Thus, a loading from 5 N to 20 N was used in the present study to cover the various hypothetical clinical scenarios. More information is available about the pressures exerted by the CPAP mask on the nasal bridge at unknown loading, which ranged from 60 to 75 mmHg according to one study (Brill et al., 2017), from 47 to 92 mmHg based on a second study (Brill et al., 2018), and from 84 (for optimal fitting) to 158 mmHg (at highest strap tension) according to others (Worsley et al., 2016). These values (corresponding to pressures of 6–21 kPa) were in agreement with the average contact pressures obtained in the present study in the nasal region during a loading between 5 and 20 N (which ranged from 12 to 14 kPa). Another study that applied a strap tension up to about 4 N, reported pressures at the nasal bridge from 18.6 to 32.3 mmHg (3–4 kPa) and at the zygoma from 7.7 to 18.9 mmHg (1–3 kPa) (Shikama et al., 2018), which are compatible with the 12 and 1 kPa respectively obtained in the present experiment at 5 N loading. However, at the forehead (3.3–13.2 mmHg, corresponding to 1–2 kPa), reported pressures were smaller than the 13 kPa here presented. Average contact pressure values might be more meaningful than maximum values, as peak values may be affected by force concentrations in areas with higher surface curvature (as shown by sensors saturation in the present experiment), a condition that may not adapt well if the substrate is actual human skin. On such soft substrate, increasing strap tension seems to have a significant effect on biomarker release (Worsley et al., 2016), and contact pressures greater than 5–7 kPa (40–50 mmHg) were associated to skin damage that may lead to pressure ulcers (Sugama et al., 2002). This said, the present experiment was not capable of measuring the contact pressure along the entire mask perimeter and some areas subject to loading may have been neglected. In fact, despite a general increase in contact pressure and contact pressure area from 5 to 20 N, a direct proportionality with the applied force was not evident. The distribution of the contacts may have been migrating during incremental loading – for example - toward the forehead, which central area was not included in the analysis due to a more lateral position of the sensors. In agreement with the present findings, previous authors reported similar contact pressures at the nasal bridge

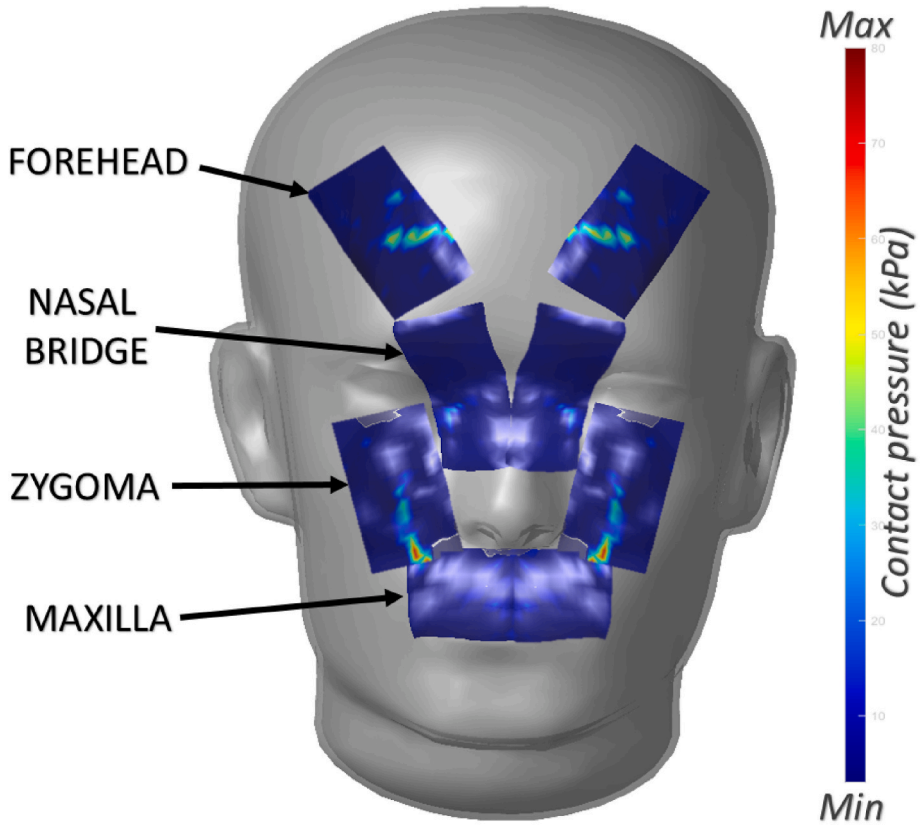

Fig. 3. Graphical representation (including mirroring of the sensors output with respect to the midline) of the peak contact pressure distributions when the CPAP mask was loaded by means of the headgear. Contact pressures are shown with a colour scale ranging from lower pressures (*blue*) to higher pressures (*red*).

by using oro-nasal masks and a slight pressure increase when a nasal mask was used, despite increased strap tension to maintain similar air leak at air pressure increasing from 15 to 25 cmH_2O (Brill et al., 2018). Other authors analysing an oro-nasal mask reported similar contact pressures on nasal bridge, maxilla, zygoma and forehead despite in the two experimental conditions (*i.e.*, with and without a personalised fitting device) the strap tension was significantly different (Shikama et al., 2018). A further work, also using an oro-nasal mask, showed increased contact pressures at the nasal bridge but similar pressures at the zygomatic region despite straps were tensioned with increments of 5 mm (Worsley et al., 2016). Overall, the experimental findings highlighted the importance of estimating the contact pressures at different anatomical areas and may suggest – for example – to prefer masks that decrease the pressures in the zygomatic region by redirecting them on forehead. In fact, forehead growth is less affected by orthopaedic forces compared to the mid-face (Savoldi et al., 2021), and forehead retrusion may have fewer consequences on nasal breathing compared to the maxillary retrusion (Lal et al., 2015). Alternatively, the design of the frame and cushion of the CPAP mask could be modified to enlarge the surface in contact with regions that are critical in terms of growth impairment or pressure ulcers formation (Lin et al., 2020). In addition, within the same anatomical region, some areas of the mask perimeter were subject to pressure concentration while others were left almost unaffected, which may be related to unwanted leakage (Kushida et al., 2008).

4.1. Limitations

The presented setup overcame a series of challenging factors. For example, the facial surface cannot be assumed to be flat for areas in the order of cm^2, and the recording allowed to transfer the sensors output matrix to the facial surface (accounting for the specific orientation and deformation). Still, the adopted head model presented evident differences with a real human skull since the facial surface was rigid and the skin layer was not simulated. These conditions represent an extremely challenging experimental problem, which can hardly be solved by a synthetic skin layer (Heo et al., 2020). In fact, sensors such as the one adopted in the present study are relatively rigid, and their use on artificial skin or even on real patients (Brill et al. 2017, 2018) may have limitations as their rigidity would conflict with the presence of a softer substrate. Hence, approaches via numerical simulation such as FEA may be valuable to achieve meaningful estimations of the effects related to the presence of soft tissue (Genna, 2022). In this picture, although the measurements we performed in this experimental study may overestimate the real ones, the information about pressure distribution can provide useful hints in mask design. Furthermore, the skull was a single piece, while the real human skull is composed by separate bones. This said, although skull models with craniofacial sutures are commercially available (Khalid, 2018), the 2–12 N force capable of generating clinical bone remodelling when applied over a period of months, is – instead – incapable to deform a human skull when applied just for seconds or minutes. In addition, a series of variables may affect the distribution of the pressures of the CPAP mask on the face, such as the mask size, type, and orientation of the headgear straps securing it on the calvaria (Tanne and Matsubara, 1996). In addition, the present case study considered a single face shape, while mask goodness of fit vary among individuals (Verberne et al., 2020). Furthermore, it is noteworthy that no air pressure was applied (*i.e.*, the CPAP mask was not tested during connection with a CPAP machine), which may affect the overall contact pressure distribution. Several of these aspects might be overly challenging for an experimental approach. Therefore, modelling and simulation might be advisable (Genna et al., 2022; Tanne and Matsubara, 1996) for including the coupling of solid and fluid dynamics (Wakayama et al., 2016) and for introducing the temporal bone remodelling. Finally, focusing on the

clinical impact of the present work, it is noteworthy that the present study did not aim at suggesting clinical guidelines for the use of CPAP masks, and the presented results should be interpreted with caution when related to clinical decision making.

5. Conclusions

- The presented experimental model may be used for providing an overall estimation of the contact pressures applied via the CPAP mask on the face of a prototypical subject.
- CPAP masks create contact pressures that are not uniformly distributed on the face, and the design of their frame, cushion, and headgear should be oriented to re-distribute such pressures towards anatomical areas with lower risk of deformation or soft tissue injury.
- Within the limitations of this study, the presented findings may be considered by clinicians and technologists for obtaining a good compromise between delivering the best treatment (in terms of ventilation) and reducing the side-effects on living tissues.

Funding

This research did not receive any specific grant from funding agencies in the public, commercial, or not-for-profit sectors.

CRediT authorship contribution statement

Fabio Savoldi: Writing – review & editing, Writing – original draft, Project administration, Methodology, Investigation, Formal analysis, Conceptualization. **Lorenzo Svanetti:** Writing – original draft, Methodology, Investigation. **James K.H. Tsoi:** Writing – review & editing, Resources, Methodology. **Min Gu:** Writing – review & editing, Resources, Methodology. **Corrado Paganelli:** Writing – review & editing, Supervision, Resources, Methodology. **Francesco Genna:** Writing – review & editing, Supervision, Methodology, Investigation. **Nicola F. Lopomo:** Writing – review & editing, Supervision, Software, Resources, Project administration, Methodology, Investigation, Formal analysis, Data curation.

Declaration of competing interest

The authors declare that they have no known competing financial interests or personal relationships that could have appeared to influence the work reported in this paper.

Acknowledgements

The authors wish to thank Prof. Antonio Fiorentino and Dr. Gabriele Allegri (Department of Mechanical and Industrial Engineering, University of Brescia, Brescia, Italy) for the support with the 3D scanning of the phantom head and the CPAP mask, and the FCI Lab (Laboratorio di Fisiologia Clinica Integrativa, University of Brescia, Brescia, Italy) for providing the contact pressure-mapping system. Part of this work was developed during the PhD thesis of Dr. Lorenzo Svanetti (Technology for Health, Department of Information Engineering, University of Brescia, Brescia, Italy).

APPENDIX

Acquisition of facial surface and sensors position:

Information about facial surface, sensors surface (as they were deformed to adhere to the facial surface), and sensors position were acquired as point-cloud non-structured information. Such information was aligned with the 3D head via a rigid registration procedure (Iterative Closest Point Alignment) using a commercial software (MeshLab, ISTI - CNR Research Center, Italy). These acquisitions allowed to transfer the output of the sensors matrix onto the facial surface (accounting for the specific orientation and deformation). In order to obtain this information, a mesh model of a sensor was created with a software (Blender, Blender Foundation, Netherlands), where each vertex of the 11×22 mesh represented a sensible element of the sensor. The mesh was adapted to the point-cloud acquired for each sensor through morphing tools (Sculping, Blender, Blender Foundation, Netherlands).

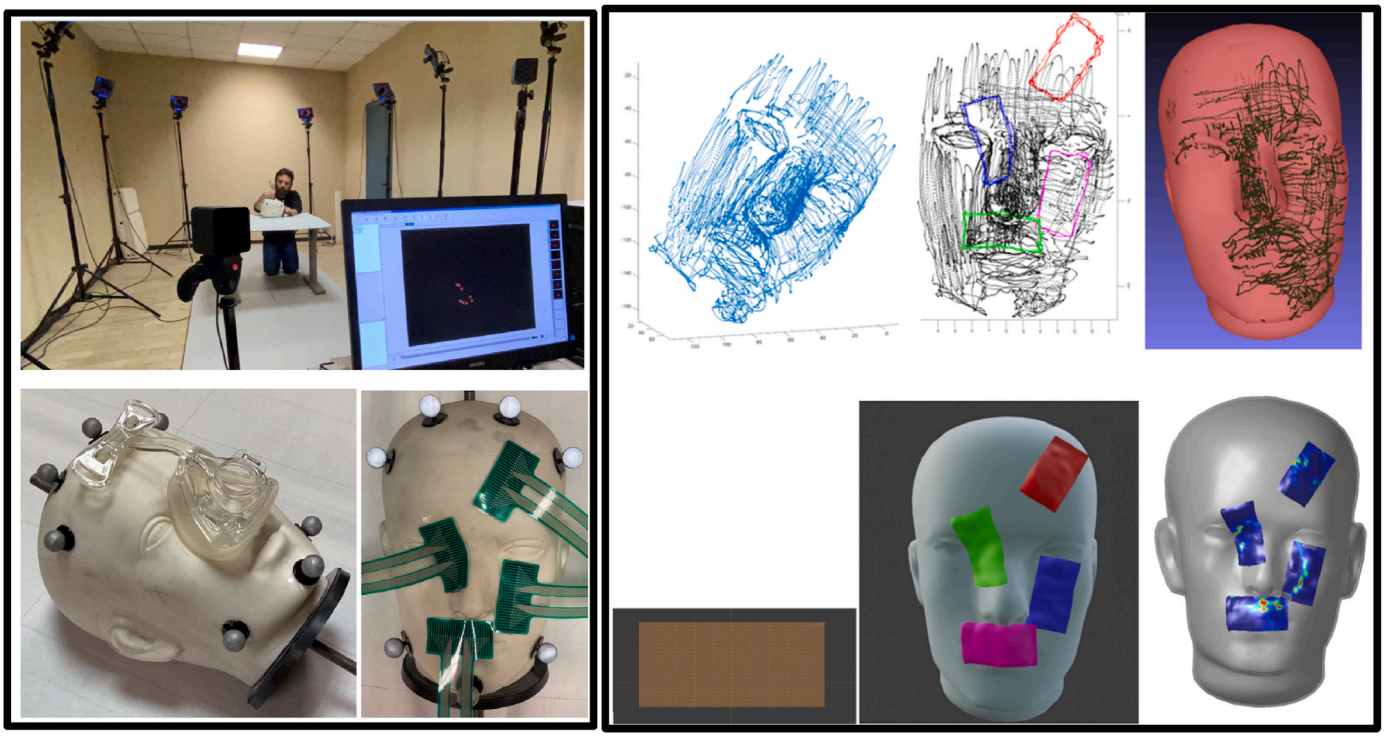

Appendix Fig. 1. Acquisition of the 3D position of the sensors on the phantom head with reflective markers applied (*left*). Acquisition of the 3D point-cloud surfaces by optoelectronic system with details of the facial surface, the four contact pressure mapping sensors, the mesh of a single pressure sensor, the position of the mesh of each of the four sensors on the 3D model of the head, and an example of pressure mapping obtained on the four sensors (*right*).

Calibration of sensors:

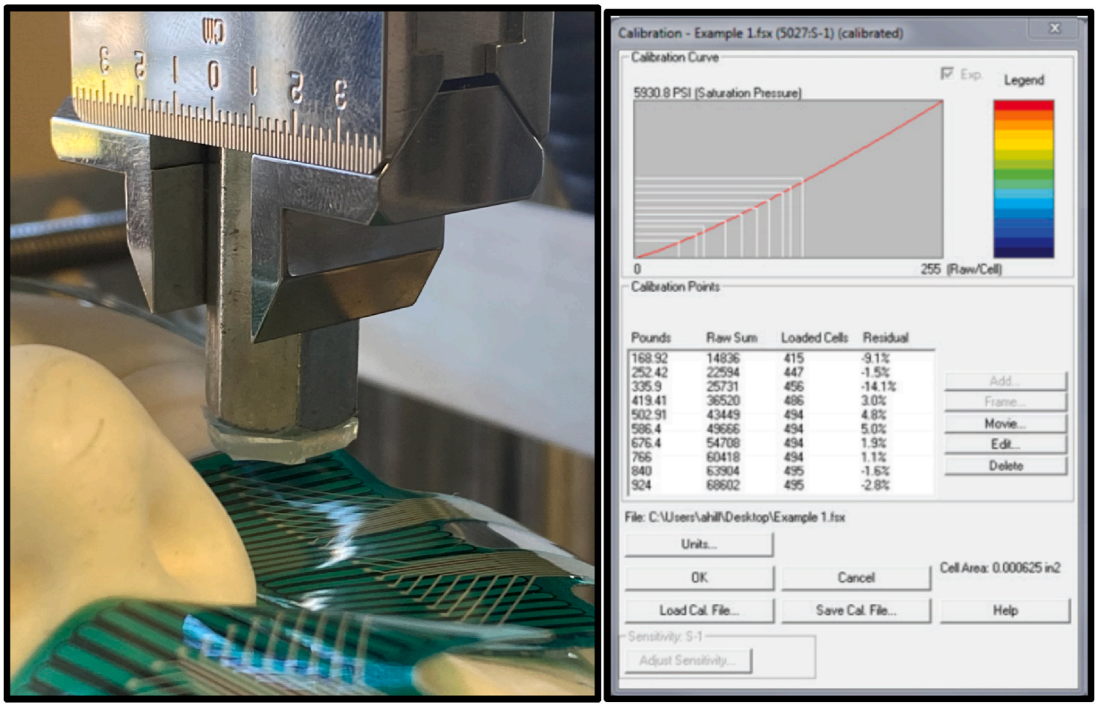

Appendix Fig. 2. Detail of the calibration of one sensor using the mechanical testing machine.

Output limits of sensors:

Appendix Table 1
Number of saturated elements (sensels) for each sensor, out of a total of 264 elements. Peak contact pressures (kPa) are reported, where values indicated with ">" corresponding to the peak saturation pressure of the specific sensor.

Region	Number of saturated elements (sensels)				Peak contact pressure [kPa]			
	5 N	10 N	15 N	20 N	5 N	10 N	15 N	20 N
Forehead	2	2	0	1	>54.6067	>54.6067	52.00	>54.6067
Zygoma	2	3	3	3	>68.8254	>68.8254	>68.8254	>68.8254
Nasal bridge	0	0	0	0	22.00	23.00	23.00	23.00
Maxilla	2	3	4	6	>22.7826	>22.7826	>22.7826	>22.7826

Mechanical testing of CPAP mask with perpendicular forces:

A series of tests was performed by applying a direct perpendicular force of 20 N on the mask with the head positioned face-up and the mask on top. Force was applied through a SS sphere (Ø = 25.4 mm) that was positioned in the anterior hole of the mask (used for the pipe connection), so that a purely axial load and uniform stress were present. These settings were adopted to have a simplified model that was used for validation of the finite element analysis (FEA) model.

Appendix Fig. 3. Setup for the mechanical testing with the CPAP directly loaded with perpendicular forces via the mechanical testing machine.

Mechanical testing of CPAP materials:

Additional tests were also performed for the mechanical characterisation of the materials that was necessary for creating the FEA model. A CPAP mask (which was the same model of the scanned mask) was used for the preparation of the specimens. Tests were performed measuring time (s), displacement (mm), and force (N) under imposed displacement. All materials showed a linear stress/strain relationship from 0 to 20 N. The polycarbonate under compression showed Young's modulus of 226 MPa, the polycarbonate under tension a modulus of 1190 MPa, the thin silicone

specimen under tension a modulus of 1.27 MPa, the thick silicone specimen under tension a modulus of 1.31 MPa, the short neoprene/nylon bend under tension a modulus of 1.66 MPa, and the long neoprene/nylon bend under tension a modulus of 1.38 MPa.

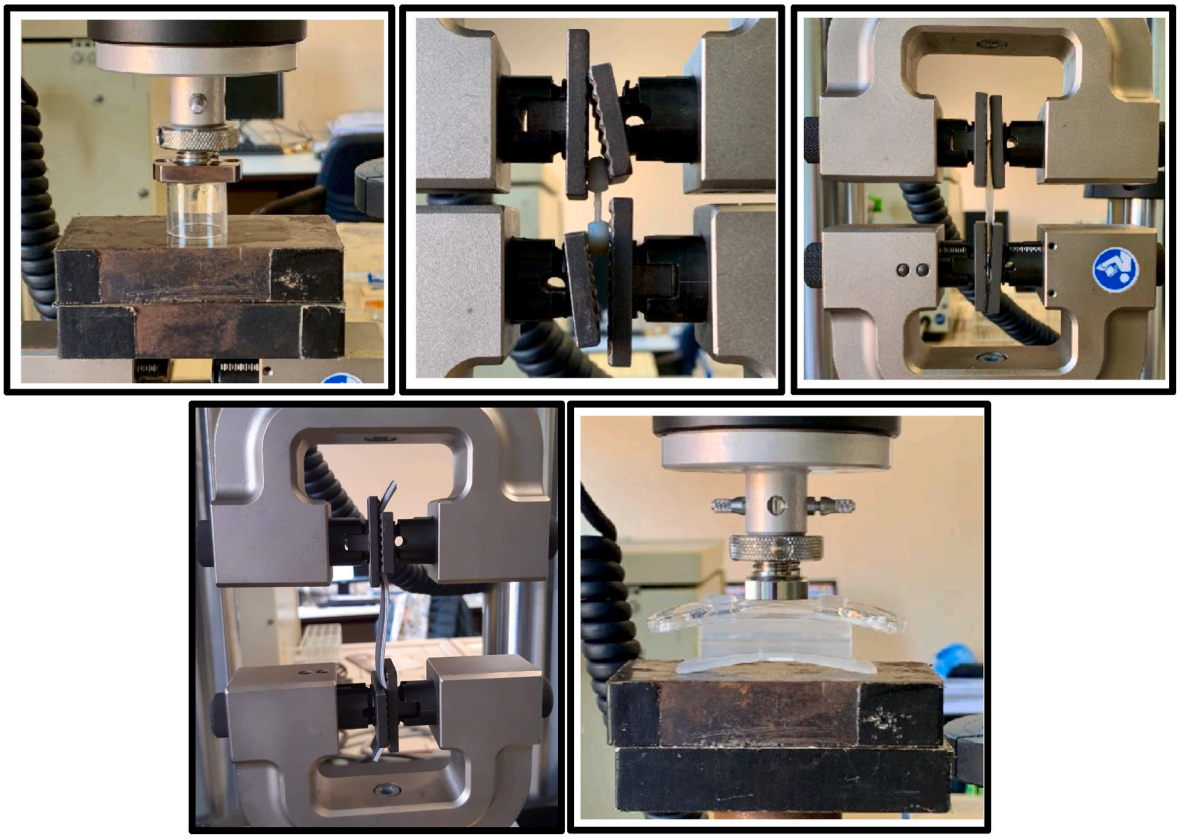

Appendix Fig. 4. Material testing of polycarbonate (A and B), silicone (C), headgear straps (D), and polycarbonate-silicone structure forming the forehead support (E).

References

Braun, S., Bottrel, J.A., 2004. Pilot study evaluating the effects of a cervical headgear on the c-axis: the growth axis of the dentomaxillary complex. Am. J. Orthod. Dentofacial Orthop. 126 (6), 694–698.

Brill, A.K., Moghal, M., Morrell, M.J., Simonds, A.K., 2017. Randomized crossover trial of a pressure sensing visual feedback system to improve mask fitting in noninvasive ventilation. Respirology 22 (7), 1343–1349.

Brill, A.K., Pickersgill, R., Moghal, M., Morrell, M.J., Simonds, A.K., 2018. Mask pressure effects on the nasal bridge during short-term noninvasive ventilation. ERJ Open Res. 4 (2).

Brimacombe, J.M., Wilson, D.R., Hodgson, A.J., Ho, K.C., Anglin, C., 2009. Effect of calibration method on tekscan sensor accuracy. J. Biomech. Eng. 131 (3), 34503.

Bushby, K.M., Cole, T., Matthews, J.N., Goodship, J.A., 1992. Centiles for adult head circumference. Arch. Dis. Child. 67 (10), 1286–1287.

Carron, M., Freo, U., BaHammam, A.S., Dellweg, D., Guarracino, F., Cosentini, R., Feltracco, P., Vianello, A., Ori, C., Esquinas, A., 2013. Complications of non-invasive ventilation techniques: a comprehensive qualitative review of randomized trials. Br. J. Anaesth. 110 (6), 896–914.

Fauroux, B., Lavis, J.F., Nicot, F., Picard, A., Boelle, P.Y., Clement, A., Vazquez, M.P., 2005. Facial side effects during noninvasive positive pressure ventilation in children. Intensive Care Med. 31 (7), 965–969.

Fischer, H.S., Roehr, C.C., Proquitte, H., Wauer, R.R., Schmalisch, G., 2008. Assessment of volume and leak measurements during cpap using a neonatal lung model. Physiol. Meas. 29 (1), 95–107.

Garlet, T.P., Coelho, U., Repeke, C.E., Silva, J.S., Cunha Fde, Q., Garlet, G.P., 2008. Differential expression of osteoblast and osteoclast chemmoatractants in compression and tension sides during orthodontic movement. Cytokine 42 (3), 330–335.

Gefen, A., Alves, P., Ciprandi, G., Coyer, F., Milne, C.T., Ousey, K., Ohura, N., Waters, N., Worsley, P., 2020. Device-related pressure ulcers: secure prevention. J. Wound Care 29 (Suppl. 2a), S1–S52.

Gefen, A., Ousey, K., 2020. Update to device-related pressure ulcers: secure prevention. Covid-19, face masks and skin damage. J. Wound Care 29 (5), 245–259.

Genna, F., 2022. Numerical analysis of the mechanical behavior of cpap masks: effects of modelling the soft tissues. J. Mech. Mater. Struct. (in press).

Genna, F., Lopomo, N.F., Savoldi, F., 2022. Validation of a numerical model for the mechanical behavior of a continuous positive airway pressure mask. Comput. Methods Biomech. Biomed. Eng. 25 (2), 165–175.

Graber, T.M., Rakosi, T., Petrovic, A.G., 1985. Dentofacial Orthopedics with Functional Appliances. Mosby, St. Louis.

Gu, M., Savoldi, F., Chan, E.Y.L., Tse, C.S.K., Lau, M.T.W., Wey, M.C., Hagg, U., Yang, Y., 2021. Changes in the upper airway, hyoid bone and craniofacial morphology between patients treated with headgear activator and herbst appliance: a retrospective study on lateral cephalometry. Orthod. Craniofac. Res. 24 (3), 360–369.

Heo, S.H., Kim, C., Kim, T.S., Park, H.S., 2020. Human-palm-inspired artificial skin material enhances operational functionality of hand manipulation. Adv. Funct. Mater. 30 (25).

Hierl, T., Kloppel, R., Hemprich, A., 2001. Midfacial distraction osteogenesis without major osteotomies: a report on the first clinical application. Plast. Reconstr. Surg. 108 (6), 1667–1672.

Ho, S.P., Marshall, S.J., Ryder, M.I., Marshall, G.W., 2007. The tooth attachment mechanism defined by structure, chemical composition and mechanical properties of collagen fibers in the periodontium. Biomaterials 28 (35), 5238–5245.

Jennum, P., Riha, R.L., 2009. Epidemiology of sleep apnoea/hypopnoea syndrome and sleep-disordered breathing. Eur. Respir. J. 33 (4), 907–914.

Johnson, P.D., Bar-Zion, Y., Taylor, M., Wheeler, T.T., 1999. Effects of head posture on headgear force application. J. Clin. Orthod. 33 (2), 94–97.

Khalid, G.A., 2018. A Coupled Physical – Computational Methodology for the Investigation of Short Fall Related Infant Head Impact. Cardiff University.

Krieger, J., 1992. Long-term compliance with nasal continuous positive airway pressure (cpap) in obstructive sleep apnea patients and nonapneic snorers. Sleep 15 (6 Suppl. l), S42–S46.

Kushida, C.A., Chediak, A., Berry, R.B., Brown, L.K., Gozal, D., Iber, C., Parthasarathy, S., Quan, S.F., Rowley, J.A., Positive Airway Pressure Titration Task F, et al., 2008. Clinical guidelines for the manual titration of positive airway pressure in patients with obstructive sleep apnea. J. Clin. Sleep Med. 4 (2), 157–171.

Lal, C., White, D.R., Joseph, J.E., van Bakergem, K., LaRosa, A., 2015. Sleep-disordered breathing in down syndrome. Chest 147 (2), 570–579.

Li, K.K., Riley, R.W., Guilleminault, C., 2000. An unreported risk in the use of home nasal continuous positive airway pressure and home nasal ventilation in children: mid-face hypoplasia. Chest 117 (3), 916–918.

Lin, H.L., Lee, Y.C., Wang, S.H., Chiang, L.Y., Liu, J.F., 2020. In vitro evaluation of facial pressure and air leak with a newly designed cushion for non-invasive ventilation masks. Healthcare 8 (4).
Lumeng, J.C., Chervin, R.D., 2008. Epidemiology of pediatric obstructive sleep apnea. Proc. Am. Thorac. Soc. 5 (2), 242–252.
Lyons, E.K., Ramsay, D.S., 2002. Preliminary tests of a new device to monitor orthodontic headgear use. Semin. Orthod. 8 (1), 29–34.
Ma, Z., Drinnan, M., Hyde, P., Munguia, J., 2018. Mask interface for continuous positive airway pressure therapy: selection and design considerations. Expet Rev. Med. Dev. 15 (10), 725–733.
McArdle, N., Devereux, G., Heidarnejad, H., Engleman, H.M., Mackay, T.W., Douglas, N. J., 1999. Long-term use of cpap therapy for sleep apnea/hypopnea syndrome. Am. J. Respir. Crit. Care Med. 159 (4 Pt 1), 1108–1114.
Nightingale, R., Nwosu, N., Kutubudin, F., Fletcher, T., Lewis, J., Frost, F., Haigh, K., Robinson, R., Kumar, A., Jones, G., et al., 2020. Is continuous positive airway pressure (cpap) a new standard of care for type 1 respiratory failure in covid-19 patients? A retrospective observational study of a dedicated covid-19 cpap service. BMJ Open Respir. Res. 7 (1).
Ochoa, B.K., Nanda, R.S., 2004. Comparison of maxillary and mandibular growth. Am. J. Orthod. Dentofacial Orthop. 125 (2), 148–159.
Peko Cohen, L., Ovadia-Blechman, Z., Hoffer, O., Gefen, A., 2019. Dressings cut to shape alleviate facial tissue loads while using an oxygen mask. Int. Wound J. 16 (3), 813–826.
Perillo, L., Padricelli, G., Isola, G., Femiano, F., Chiodini, P., Matarese, G., 2012. Class ii malocclusion division 1: a new classification method by cephalometric analysis. Eur. J. Paediatr. Dent. 13 (3), 192–196.
Savoldi, F., Massetti, F., Tsoi, J.K.H., Matinlinna, J.P., Yeung, A.W.K., Tanaka, R., Paganelli, C., Bornstein, M.M., 2021. Anteroposterior length of the maxillary complex and its relationship with the anterior cranial base. Angle Orthod. 91 (1), 88–97.
Savoldi, F., Tsoi, J.K.H., Paganelli, C., Matinlinna, J.P., 2018. The biomechanical properties of human craniofacial sutures and relevant variables in sutural distraction osteogenesis: a critical review. Tissue Eng. B Rev. 24 (1), 25–36.
Schallom, M., Cracchiolo, L., Falker, A., Foster, J., Hager, J., Morehouse, T., Watts, P., Weems, L., Kollef, M., 2015. Pressure ulcer incidence in patients wearing nasal-oral versus full-face noninvasive ventilation masks. Am. J. Crit. Care 24 (4), 349–356 quiz 357.
Shikama, M., Nakagami, G., Noguchi, H., Mori, T., Sanada, H., 2018. Development of personalized fitting device with 3-dimensional solution for prevention of niv oronasal mask-related pressure ulcers. Respir. Care 63 (8), 1024–1032.
Sugama, J., Sanada, H., Takahashi, M., 2002. Reliability and validity of a multi-pad pressure evaluator for pressure ulcer management. J. Tissue Viability 12 (4), 148–153.
Tanne, K., Matsubara, S., 1996. Association between the direction of orthopedic headgear force and sutural responses in the nasomaxillary complex. Angle Orthod. 66 (2), 125–130.
Tsuda, H., Almeida, F.R., Tsuda, T., Moritsuchi, Y., Lowe, A.A., 2010. Craniofacial changes after 2 years of nasal continuous positive airway pressure use in patients with obstructive sleep apnea. Chest 138 (4), 870–874.
Vaschetto, R., De Jong, A., Conseil, M., Galia, F., Mahul, M., Coisel, Y., Prades, A., Navalesi, P., Jaber, S., 2014. Comparative evaluation of three interfaces for non-invasive ventilation: a randomized cross-over design physiologic study on healthy volunteers. Crit. Care 18 (1), R2.
Verberne, J.W.R., Worsley, P.R., Bader, D.L., 2020. A 3d registration methodology to evaluate the goodness of fit at the individual-respiratory mask interface. Comput. Methods Biomech. Biomed. Eng. 1–12.
Villa, M.P., Pagani, J., Ambrosio, R., Ronchetti, R., Bernkopf, E., 2002. Mid-face hypoplasia after long-term nasal ventilation. Am. J. Respir. Crit. Care Med. 166 (8), 1142–1143.
Wakayama, T., Suzuki, M., Tanuma, T., 2016. Effect of nasal obstruction on continuous positive airway pressure treatment: computational fluid dynamics analyses. PLoS One 11 (3), e0150951.
Worsley, P.R., Prudden, G., Gower, G., Bader, D.L., 2016. Investigating the effects of strap tension during non-invasive ventilation mask application: a combined biomechanical and biomarker approach. Med. Dev. 9, 409–417.
Yamaguti, W.P., Moderno, E.V., Yamashita, S.Y., Gomes, T.G., Maida, A.L., Kondo, C.S., de Salles, I.C., de Brito, C.M., 2014. Treatment-related risk factors for development of skin breakdown in subjects with acute respiratory failure undergoing noninvasive ventilation or cpap. Respir. Care 59 (10), 1530–1536.